


## Article

# Exploring the Effect of Hierarchical Porosity in BEA Zeolite in Friedel-Crafts Acylation of Furan and Benzofuran

Nelson Nunes <sup>1,2,\*</sup> , Ana P. Carvalho <sup>2,3</sup>, Ruben Elvas-Leitão <sup>1,2</sup> , Filomena Martins <sup>2,3</sup>, Auguste Fernandes <sup>4</sup>, João Rocha <sup>5</sup> and Angela Martins <sup>1,2,\*</sup> 

- <sup>1</sup> Departamento de Engenharia Química, Instituto Superior de Engenharia de Lisboa, Instituto Politécnico de Lisboa, Rua Conselheiro Emídio Navarro, 1959-007 Lisboa, Portugal
- <sup>2</sup> Centro de Química Estrutural, Institute of Molecular Sciences, Faculdade de Ciências, Universidade de Lisboa, Ed. C8, Campo Grande, 1749-016 Lisboa, Portugal
- <sup>3</sup> Departamento de Química e Bioquímica, Faculdade de Ciências, Universidade de Lisboa, Ed. C8, Campo Grande, 1749-016 Lisboa, Portugal
- <sup>4</sup> Centro de Química Estrutural, Institute of Molecular Sciences, Instituto Superior Técnico, Universidade de Lisboa, Ed. C8, Campo Grande, 1749-016 Lisboa, Portugal
- <sup>5</sup> Departamento de Química and CICECO, Universidade de Aveiro, 3810-193 Aveiro, Portugal
- \* Correspondence: nnunes@deq.isel.ipl.pt (N.N.); amartins@deq.isel.ipl.pt (A.M.)

**Abstract:** Hierarchical BEA zeolite was prepared through desilication or desilication followed by acid treatment. The catalytic performance of BEA zeolite samples was evaluated using Friedel-Crafts acylations with two substrates of different molecular sizes, furan (5.7 Å) and benzofuran (6.9 Å), in the presence of acetic anhydride as acylating agent. The application of the simplified Langmuir-Hinshelwood kinetic model showed that the size of the substrate leads to different catalytic activities, with improved rate constant and turnover frequency (TOF) solely in the presence of benzofuran for both desilicated and further acid treated samples. The mesopores developed during the zeolite treatments have an important role as transportation channels by reducing diffusion limitations. The application of Quantitative Structure–Property Relationships (QSPR) allowed the finding of the most relevant properties of the zeolite and substrate with impact on the catalytic parameters.

**Keywords:** hierarchical BEA; Friedel-Crafts acylation; furan; benzofuran; kinetic modelling; QSPR analysis



**Citation:** Nunes, N.; Carvalho, A.P.; Elvas-Leitão, R.; Martins, F.; Fernandes, A.; Rocha, J.; Martins, A. Exploring the Effect of Hierarchical Porosity in BEA Zeolite in Friedel-Crafts Acylation of Furan and Benzofuran. *Catalysts* **2022**, *12*, 1064. <https://doi.org/10.3390/catal12091064>

Academic Editor: Antonio Eduardo Palomares

Received: 17 August 2022

Accepted: 15 September 2022

Published: 17 September 2022

**Publisher's Note:** MDPI stays neutral with regard to jurisdictional claims in published maps and institutional affiliations.



**Copyright:** © 2022 by the authors. Licensee MDPI, Basel, Switzerland. This article is an open access article distributed under the terms and conditions of the Creative Commons Attribution (CC BY) license (<https://creativecommons.org/licenses/by/4.0/>).

## 1. Introduction

Friedel-Crafts reactions are among the best-known types of transformations of aromatic molecules. The name of these reactions derived from two chemists, named Charles Friedel and James Mason Crafts, who first studied these reactions around 1877 [1]. Typically, at the industrial level, these reactions occur in the presence of homogeneous catalysts such as  $\text{AlCl}_3$  or HF, with associated disposal problems. Quite often, separation and recovery are difficult. Several studies reported the use of alternative solid catalysts in liquid phase reactions [2,3]. Zeolites are solid materials with a unique combination of properties such as high surface area, well defined porosity, intrinsic acidity as well as high thermal and mechanical stability [4]. The application of zeolites in Friedel-Crafts acylation reactions have been reviewed by Clerici [5], Sartori and Maggi [6], Liang et al., [7] and, more recently, Nayak et al. [8]. In all cases, BEA (commercially known as Beta zeolite) and FAU (known as Y zeolite) are the most explored structures. It is also worth mentioning that commercial scale processes for the acylation of aromatic compounds (with acetic anhydride) have already been developed by Rhône-Poulenc (now Rhodia) using the BEA zeolite structure [9]. However, the purely microporous nature of zeolites has been reported as a drawback since the narrow pore apertures limit the diffusion of large molecules towards the inner active sites, which are also the most interesting ones from the perspective of industrial applications. The development of hierarchical zeolites, with mesoporosity in addition to

the native micropores, seems to be a good strategy to improve accessibility and overcome the diffusion limitations [10]. The following two main strategies were attempted to attain this purpose: (i) synthesis of nano-sized crystals [11,12] that lead to gains in the external surface area, exposing a high number of pore openings that causes a fast desorption of large products; (ii) post-synthesis treatments such as desilication, using alkaline solutions such as NaOH. By changing the experimental conditions, namely the concentration of the alkali, temperature, and duration of the treatments, tuned mesoporosity can be achieved with improved catalytic performance [13]. However, as desilication treatments may also lead to the deposition of extra-framework Al species [14,15], an additional acid treatment is recommended to remove the debris. This strategy was widely used by Verboekend and co-workers [16] in their studies focused on MFI (also known as ZSM-5) zeolites. The same procedure was applied by other authors to other zeolite structures, some of which were used as heterogeneous catalysts in Friedel-Crafts reactions. For example, Wang et al. [17] modified BEA zeolite through an alkaline treatment with NaOH followed by acid leaching with HNO<sub>3</sub>. The characterization of the modified samples showed that, under the tested operational conditions, the mesoporosity was developed mainly through crystal aggregation. This feature caused some improvement in the Friedel-Crafts alkylation of mesitylene with benzyl alcohol since the large size of the substrate, and the respective reaction intermediates, lead to the occurrence of catalytic transformations mainly at the created intercrystalline mesopores. An identical methodology was followed by us in previous works [18,19], but our purpose was to use mild desilication or desilication and acid leaching conditions to develop intracrystalline mesoporosity and study its influence on Friedel-Crafts acylation of small substrates such as furan, pyrrole, and anisole with acetic anhydride as acylating agent. In all these studies, Quantitative Structure–Property Relationships (QSPR) were applied to rationalize which changes in the substrates' characteristics (size, polarity, etc.) had more influence on the improvement of the catalytic behavior of Friedel-Crafts reactions in heterogeneous media. In the mentioned studies, hierarchical MWW (also known as MCM-22) [18] and BEA [19,20] materials were desilicated using 0.1 M NaOH solution followed, in some cases, by an acid treatment with 0.1 M HCl solution. In both cases, it was found that the desilication treatment, especially when followed by acid washing, caused an increase in product yield and rate constant. For the BEA structure, the application of kinetic models using nonlinear regressions showed that the Si/Al ratio of the parent materials had a strong influence on the catalytic behavior [19]. More recently, we enlarged the number of substrates, including substrates of different sizes and functionalities, and found that the mild conditions used to prepare the hierarchical catalyst did not lead to an increase in rate constant and product yield in the presence of large molecules such as benzofuran and benzothiophen [20]. In this context, the purpose of this study was to prepare hierarchical BEA zeolite through post-synthesis desilication followed by acid treatment, using the same strategy as before, but now, by using higher NaOH concentrations, we intend to tune the mesoporosity so that it enhances the catalytic performance in the presence of a larger substrate such as benzofuran. In line with our previous works [18–20], a Langmuir-Hinshelwood model was applied to quantify the catalytic parameters of the reaction and a multiple linear regression (MLR)-based QSPR methodology was used to find and quantify the combined effect of modifying both zeolite and substrate properties.

## 2. Results and Discussion

### 2.1. Materials Characterization

BEA zeolite (Si/Al ratio = 12.5) was subjected to alkaline treatment with 0.2 or 0.4 M NaOH solutions at 60 °C for 30 min and, in some cases, it was followed by an acid washing with 0.1 M HCl at 70 °C for 3 h. The samples were labeled as BEA<sub>x</sub>, where *x* is the NaOH concentration, followed by AT in the case of acid treated materials. The X-ray powder diffraction patterns of parent and modified samples, and the N<sub>2</sub> adsorption isotherms at −196 °C were presented in a previous work [21]. The degree of crystallinity (%) of the modified samples, *C*<sub>XRD</sub>, estimated based on the area of the peak at 2θ around 22° ,

taking parent BEA as reference, and the textural parameters obtained from N<sub>2</sub> isotherms are summarized in Table 1 and commented in brief.

**Table 1.** Degree of crystallinity, C<sub>XRD</sub>, textural parameters, and Brønsted [B]<sub>pyr</sub> and Lewis [L]<sub>pyr</sub> acid sites concentration.

Catalyst	C <sub>XRD</sub> <sup>1</sup> (%)	V <sub>micro</sub> <sup>2</sup> (cm <sup>3</sup> g <sup>-1</sup> )	V <sub>meso</sub> <sup>2</sup> (cm <sup>3</sup> g <sup>-1</sup> )	A <sub>ext</sub> <sup>2</sup> (m <sup>2</sup> g <sup>-1</sup> )	[B] <sub>pyr</sub> <sup>3</sup> (mmol g <sup>-1</sup> )		[L] <sub>pyr</sub> <sup>3</sup> (mmol g <sup>-1</sup> )	
					T =150 °C	T =350 °C	T =150 °C	T =350 °C
BEA	100	0.17	0.40	246	0.225	0.078	0.273	0.212
BEA0.2	87	0.13	0.42	211	0.238	0.105	0.231	0.176
BEA0.2AT	90	0.15	0.49	237	0.208	0.112	0.093	0.090
BEA0.4	76	0.12	0.43	191	0.237	0.087	0.230	0.172
BEA0.4AT	74	0.13	0.48	190	0.243	0.101	0.143	0.129

<sup>1</sup> Calculated from powder X-ray diffraction patterns, taking parent BEA as reference. <sup>2</sup> Textural parameters quantified from low temperature N<sub>2</sub> adsorption isotherms: V<sub>micro</sub> (micropore volume), V<sub>meso</sub> (mesopore volume), and A<sub>ext</sub> (external surface area). <sup>3</sup> Values estimated from pyridine adsorption followed by FTIR, after pyridine adsorption at room temperature upon heat treatment at 150 °C and 350 °C for 1.5 h.

As can be observed from the C<sub>XRD</sub> values, shown in Table 1, as the severity of basic treatment increased from 0.2 to 0.4 M NaOH, a decrease in C<sub>XRD</sub> occurs, being more pronounced for the BEA0.4 sample, as expected. Upon acid washing with HCl, no significant changes in C<sub>XRD</sub> are observed when compared to the samples submitted solely to the alkaline treatment.

The textural properties were evaluated through the analysis of the N<sub>2</sub> adsorption isotherms measured at −196 °C and are shown in Table 1. The desilication step resulted in some decrease in V<sub>micro</sub> regardless of the concentration of the NaOH solution used, which can be attributed to some deposition of extra-framework species leading to the partial obstruction of the micropores. The acid treatment promoted the recovery of some V<sub>micro</sub> due to the leaching of extra-framework debris, especially in the case of the BEA0.2AT sample. The development of mesoporosity was achieved for the two desilicated samples and deepened upon acid leaching. However, for the acid treated samples, no significant gain was verified in V<sub>meso</sub> when the base concentration was increased from 0.2 to 0.4 M, although the value reached (0.49 cm<sup>3</sup> g<sup>-1</sup> for BEA0.2AT, and 0.48 cm<sup>3</sup> g<sup>-1</sup> for BEA0.4AT) was higher than the one obtained for the samples treated with 0.1 M NaOH reported in our previous study (0.44 cm<sup>3</sup> g<sup>-1</sup>) [19]. Concerning the mesopore size distribution (Figure S1), for all samples, most pores' apertures lie in the range 10–20 nm, but as the base concentration increased from 0.2 to 0.4 M, there was a progressive enlargement of the pores' width greater than 20 nm, which was more evident in the BEA0.4AT sample.

The <sup>29</sup>Si MAS-NMR spectra of parent and modified samples, presented in Figure 1 left, show an intense broad peak at around −111 ppm with a shoulder at ca. −114 ppm ascribed to two distinct crystallographic Si(OSi)<sub>4</sub> environments (Q<sup>4</sup> sites). A weak peak at ca. −103 ppm is attributed to Si(OH)(OSi)<sub>3</sub> environments (Q<sup>3</sup> sites), and a very weak resonance at ca. 92 ppm points to the presence of Si(OH)<sub>2</sub>(OSi)<sub>2</sub> (Q<sup>2</sup> sites). It must be stressed that these attributions were made based on our previous studies on cross-polarization for BEA samples desilicated with 0.1 M NaOH solution [19]. To gain a deeper understanding on the structural changes caused by the post-synthesis modifications of the BEA structure, the relative amount of Q<sup>n</sup> sites were estimated by fitting the spectra with Gaussian functions using Peak-Fit software.

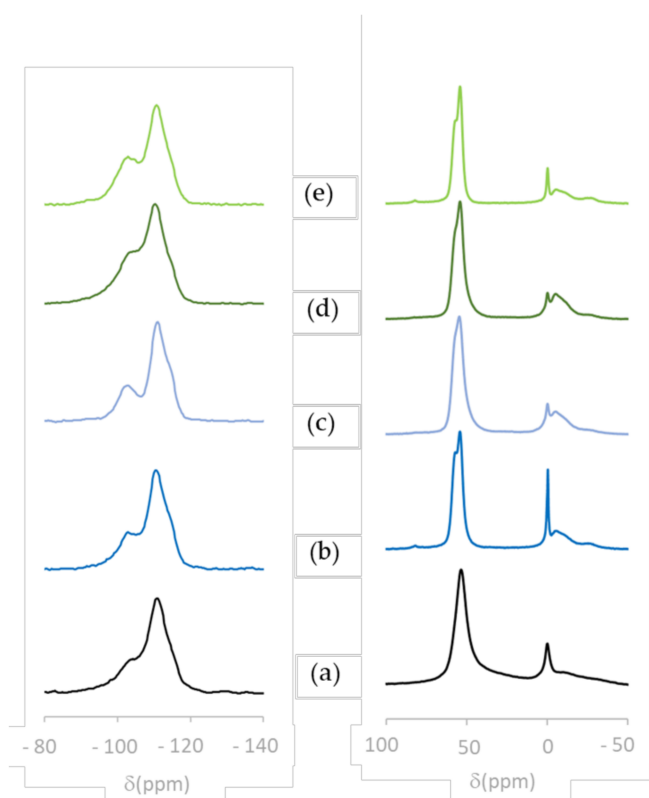


**Figure 1.**  $^{29}\text{Si}$  MAS-NMR (left) and  $^{27}\text{Al}$  MAS-NMR (right) spectra of parent and modified samples. (a) BEA; (b) BEA0.2; (c) BEA0.2AT; (d) BEA0.4; (e) BEA0.4AT.

The results listed in Table 2 show that for all samples  $\text{Q}^4$  sites prevail over  $\text{Q}^3$  and  $\text{Q}^2$  sites. The NaOH treatment resulted in the removal of Si atoms from  $\text{Q}^4$  positions, which becomes more pronounced with the increase in NaOH concentration. A small increase in  $\text{Q}^3$  species is in accordance with previous studies by Wang et al. [17]. On the other hand, an increase in  $\text{Q}^2$  positions, ascribed to SiOH groups, is attributed to the presence of silanol groups on the mesopore walls [17]. Upon acid treatment, there is almost no change in the Si amount at  $\text{Q}^2$  environments. An increase in the relative amount of  $\text{Q}^4$  sites as well as a decrease in  $\text{Q}^3$  sites was noticed. This is attributed to some partial removal of Al during the acid treatment and is due to the fragility of the zeolite structure upon treatment with NaOH.

**Table 2.** Relative amount (expressed in %) of  $\text{Q}^n$  ( $n = 4-2$ ) sites ascertained from  $^{29}\text{Si}$ MAS-NMR and tetrahedral-to-octahedral Al ratio ( $\text{Al}_{\text{tet}}/\text{Al}_{\text{oct}}$ ) determined from  $^{27}\text{Al}$  MAS-NMR.

Catalyst	$\text{Q}^4$	$\text{Q}^3$	$\text{Q}^2$	$\text{Al}_{\text{tet}}/\text{Al}_{\text{oct}}$
BEA	57	33	9	2.4
BEA0.2	53	35	11	2.3
BEA0.2AT	56	32	12	2.7
BEA0.4	50	37	11	2.1
BEA0.4AT	54	35	11	3.1

The  $^{27}\text{Al}$  MAS-NMR spectra in Figure 1 right, show peaks located around 54–58 ppm ascribed to tetrahedral Al species and two peaks attributed to octahedral Al: a sharp one located at ca. 0 ppm and a broad one at ca. –5 ppm. The parent BEA sample contains a significant amount of extra-framework aluminum denoted by the peaks ascribed to Al in the octahedral position, which is not surprising due to the defects typically present on the BEA zeolite structure. The ratio between the integrated areas of the peak ascribed

to tetrahedral positions and those attributed to octahedral sites ( $Al_{tet}/Al_{oct}$ ), estimated using Peak-Fit software, is also presented in Table 2. As can be observed, the desilication process led to a slight decrease in  $Al_{tet}/Al_{oct}$ . This is due to the removal of framework Si leading to the accumulation of extra-framework Al owing to the treatment with NaOH. This effect is more pronounced in the case of BEA0.4 catalyst. In both cases, the acid treatment promotes the removal of extra-framework Al, in line with the values obtained for the textural parameters where some recovery of  $V_{micro}$  and the increase in  $V_{meso}$  are noted (see Table 1).

The infrared spectra for the adsorption of pyridine on Brönsted (B) and Lewis (L) acid sites in the spectral region 1300–1700  $cm^{-1}$  upon degassing at 150 °C and 350 °C are shown in Figure 2. The characteristic bands attributed to pyridine adsorbed on Brönsted (B) sites,  $PyH^+$  at around 1545  $cm^{-1}$ , and to Lewis (L) sites,  $PyL$ , at about 1455  $cm^{-1}$ , were observed. In addition, an intense and sharp band located at 1490  $cm^{-1}$  is observed in all the cases, which is ascribed to pyridine adsorbed on both types of acid sites. Table 1 presents the acid sites concentration ( $[B]_{pyr}$  and  $[L]_{pyr}$ ) for parent and modified BEA, estimated from the integrated area of  $PyH^+$  and  $PyL$  bands and using the molar adsorption coefficients reported in the literature [22].

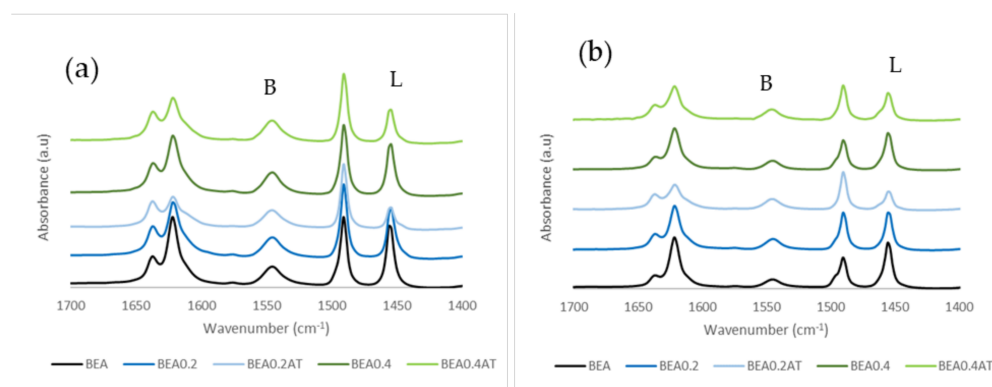


**Figure 2.** Infrared spectra of parent and treated BEA after pyridine adsorption on (B) Brönsted and (L) Lewis acid sites upon degassing at (a) 150 °C and (b) 350 °C.

The spectra displayed in Figure 2 and the acid sites concentration in Table 1 show that the parent BEA sample presents a high concentration of Brönsted acid sites, though a large part is weak since only about 35% remain upon heating at 350 °C, whereas in the case of Lewis sites almost 80% remain, meaning that they are strong acid sites. Upon alkaline treatment, a small increase in  $[B]_{pyr}$  concentration was observed, meaning that the textural modifications created due to alkaline treatments improved the accessibility of pyridine to Brönsted sites, as previously observed [19]. However, the strength of these Brönsted sites was penalized when the highest NaOH concentration was used, since only 37% of the sites remained upon heating at 350 °C for BEA0.4 against 47% for BEA0.2. In the case of Lewis acid sites, some loss of  $[L]_{pyr}$  is noted. This loss is similar and independent of the base concentration, as well as the strength of the remaining sites upon desorption at 350 °C. The acid treatment had a different effect on the two samples, namely, BEA0.2 and BEA0.4. In the case of BEA0.2AT, a decrease in both  $[B]_{pyr}$  and, especially,  $[L]_{pyr}$  at 150 °C, is noticed. In the case of BEA0.4AT, a slight increase in  $[B]_{pyr}$  compared to BEA0.4 is observed. This is a result of the increase in the mesoporosity due to the alkaline treatment of BEA followed by acid treatment (BEA0.2AT) leading to improved access of pyridine probe molecules to Brönsted acid sites. In addition, the decrease in Lewis acidity is less pronounced when compared to BEA0.2AT.

## 2.2. Results from Catalytic Reactions

The Friedel-Crafts acylation reactions were performed at 60 °C using two substrates of different sizes: a smaller molecule, furan, and a larger one, benzofuran. Based on their molar volume [20], their average diameters varied between 5.7 and 6.9 Å, which in both cases are lower than the average pore diameter of BEA zeolite [23]. In all cases, acetic anhydride was used as acylating agent. Figure 3 shows the variation in product yield as a function of reaction time for parent and treated zeolite samples. Product yields were calculated in terms of the acylated products which are always obtained in larger amounts. Although some additional products were sometimes detected, they were in very small amounts that could be attributed to the occurrence of secondary reactions. All curves in Figure 3a,b showed a similar trend, with a significant increase in product yield in the first few minutes of the reaction followed by a change in slope for reaction times greater than 10 min. A closer inspection of the curves showed a clear distinction between the results obtained with furan and benzofuran, with significantly higher product yields obtained consistently in the case of furan. It is also noted that the influence of the treatments is more expressive in the case of benzofuran, which indicates that the larger size of this molecule makes it more sensitive to the modifications performed on the catalyst.

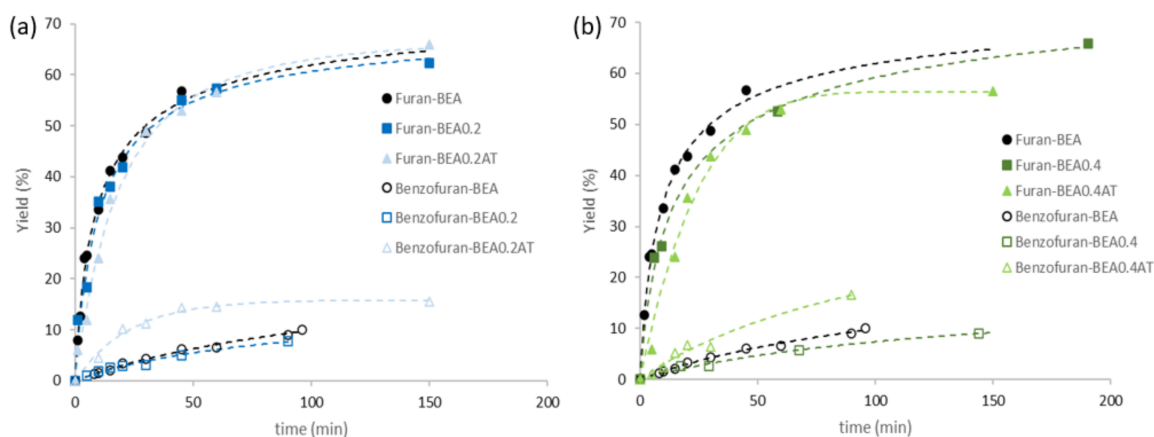


**Figure 3.** Product yield as a function of reaction time for parent and treated BEA zeolite. Effect of concentration of NaOH (a) 0.2 M and (b) 0.4 M on the desilication and catalytic activity of BEA. Full symbols for furane and empty symbols for benzofuran. (The dashed curves represent calculated values obtained from the kinetic model.).

A mathematical analysis of the results gives more insights into the effect of desilication, or desilication and acid treatment, on the Friedel-Crafts acylation of furan and benzofuran. Thus, the Langmuir-Hinshelwood model was used to determine the catalytic parameters for each reaction (see Materials and Methods). Furthermore, a QSPR analysis was performed to establish correlations between those parameters and the properties of the substrates and catalysts.

## 2.3. Kinetic Modelling

Table 3 presents the reaction rate constants ( $k$ ) and the relative sorption equilibrium constants ( $K_r$ ) obtained from the nonlinear regressions approach using the Langmuir-Hinshelwood model, as detailed in previous works [18,19], as well as the most relevant statistical information. Turnover frequencies (TOF) were estimated from the ratio of the rate constant,  $k$ , and the Brønsted acid sites concentration,  $[B]_{\text{pyr}}$  at 150 °C, according to the assumptions made by Guidotti et al. [24].



**Table 3.** Rate constants ( $k$ ), turnover frequencies (TOF), and relative sorption equilibrium constants ( $K_r$ ) of Friedel-Crafts acylation reaction of furan and benzofuran with acetic anhydride. Also presented are the fits' statistical figures of merit: determination coefficient ( $R^2$ ), regression standard deviation of fit ( $s_{\text{fit}}$ ), and Fisher-Snedecor parameter ( $F$ ).

Catalyst	Substrate	$k$ (mmol min <sup>-1</sup> g <sup>-1</sup> )	TOF (min <sup>-1</sup> )	$K_r$	$R^2$	$s_{\text{fit}}$	$F$
BEA	Furan	65 ± 2	289	8.0 ± 0.6	0.992	0.275	1021
BEA0.2	Furan	53 ± 4	222	7 ± 2	0.958	0.549	160
BEA0.2AT	Furan	26.4 ± 0.8	127	4.0 ± 0.5	0.990	0.142	710
BEA0.4	Furan	46 ± 1	194	9.1 ± 0.9	0.995	0.195	663
BEA0.4AT	Furan	17 ± 2	70	1.3 ± 0.8	0.903	0.274	56
BEA	Benzofuran	1.30 ± 0.03	5.8	25 ± 2	0.984	0.005	494
BEA0.2	Benzofuran	1.32 ± 0.06	5.5	41 ± 5	0.959	0.009	142
BEA0.2AT	Benzofuran	5.2 ± 0.6	25	33 ± 8	0.905	0.083	47
BEA0.4	Benzofuran	0.95 ± 0.06	5.0	35 ± 6	0.961	0.009	73
BEA0.4AT	Benzofuran	2.38 ± 0.08	9.8	12 ± 2	0.962	0.016	125

The analysis of the data in Table 3 shows that all nonlinear regressions exhibit good statistics (high  $R^2$  and  $F$  values and low  $s_{\text{fit}}$ ). The obtained parameters allow us to quantify some of the aspects previously discussed during the analysis of product yields vs. reaction time plots (Figure 3). As observed before, there is a huge difference in the results obtained. Concerning the smaller substrate, furan, modified catalysts display rate constants and TOF values lower than the parent BEA catalyst. In our previous study using 0.1 M NaOH to desilicate the zeolite, under the same experimental conditions reported in this work, a different behavior was noted since desilicated and acid treated samples showed an increase in  $k$  of almost 2.5 times [20]. In the present case, the only similar trend to our previous studies is the decrease in  $K_r$  for the acid treated samples indicating the fast desorption of products, hindering the occurrence of secondary reactions. For benzofuran, a different scenario is observed. Indeed, besides the low  $k$  and TOF values, an enhancement of these parameters was seen for the desilicated and acid treated samples. This is more so in the case of BEA0.2AT with a 4 time-fold increase in  $k$  and a 4.3 time-fold rise in TOF, compared to parent BEA; regarding BEA0.4AT, a more modest increase of 1.8 for  $k$  and 1.7 times for TOF is obtained. In the case of  $K_r$ , a decrease is observed only for BEA0.4AT, which can be explained attending to the larger mesopore volume present in this sample that facilitates product desorption (see Figure S1). For the substrate benzofuran, the sole desilication treatment is not enough to improve the catalytic performance probably because the debris accumulated on the external surface/pore apertures hinders the access of benzofuran to the active sites, as predicted by the analysis of textural parameters (see Table 1).

#### 2.4. Quantitative Structure-Property Relationship Analysis

The QSPR methodology was successfully applied in earlier works [18,19], in which model equations were used to correlate  $\ln k$  and  $\ln K_r$  with different zeolite and substrate properties' descriptors. Based on the number of data points, the maximum number of descriptors selected was three and the house-built excel macro [19] generated the different multiple linear regressions (MLT) combining the various descriptors, allowing the choice of the best model equation on the basis of a series of judicious statistical criteria.

In this work, the approach had to be different since the number of data points was reduced and, more importantly, because there were only two substrates. This means that there was not sufficient variability in the substrate component. Therefore, the strategy to overcome this problem was to use already published data for other substrates, using the same parent zeolite as catalyst [20]. Additionally, to try to better pinpoint the nature of substrate contributions, Abraham's solute parameters,  $V$ ,  $E$ ,  $S$ ,  $A$ , and  $B$  were also used, with  $V$  being the McGowan characteristic solute volume in units of (cm<sup>3</sup> mol<sup>-1</sup>)/100,  $E$

the solute excess molar refractivity in units of  $(\text{cm}^3 \text{mol}^{-1})/10$ , measuring the induced dipole (polarization) solute-solvent interactions,  $S$  the dipolarity/polarizability parameter reflecting the interactions associated with both induced and fixed polarity, and  $A$  and  $B$  the overall hydrogen bond donating and hydrogen bond accepting capacities, respectively [25].

Table 4 summarizes the values of the Abraham solute parameters used in this work.

**Table 4.** Substrate descriptors used in this work [25].

Substrate	$E$	$S$	$A$	$B$	$V$
Furan	0.370	0.510	0.000	0.130	0.5363
Benzofuran	0.890	0.830	0.000	0.150	0.9053
Thiophene	0.687	0.570	0.000	0.150	0.6411
Pyrrole	0.613	0.730	0.410	0.290	0.5570
Indole	1.200	1.260	0.440	0.180	0.9464
Anisole	0.710	0.750	0.000	0.290	0.9160

Table 5 shows the determination coefficients,  $r^2$ , between different descriptors.

**Table 5.** Descriptors' correlation matrix \*.

$r^2$	$C_{\text{XRD}}$	$V_{\text{micro}}$	$V_{\text{meso}}$	$A_{\text{ext}}$	$[\text{B}]_{\text{pyr}}$	$[\text{L}]_{\text{pyr}}$	$E$	$S$	$A$	$B$	$V$
$C_{\text{XRD}}$	1.0										
$V_{\text{micro}}$	<b>0.89</b>	1.0									
$V_{\text{meso}}$	0.41	0.26	1.0								
$A_{\text{ext}}$	<b>0.95</b>	<b>0.91</b>	0.21	1.0							
$[\text{B}]_{\text{pyr}}$	0.37	0.37	0.01	<b>0.58</b>	1.0						
$[\text{L}]_{\text{pyr}}$	0.30	0.20	<b>0.98</b>	0.13	0.05	1.0					
$E$	0.03	0.04	0.03	0.03	0.00	0.03	1.0				
$S$	0.04	0.05	0.03	0.04	0.01	0.03	<b>0.88</b>	1.0			
$A$	0.17	0.19	0.13	0.14	0.02	0.12	0.13	0.33	1.0		
$B$	0.23	0.25	0.17	0.19	0.03	0.16	0.05	0.08	0.28	1.0	
$V$	0.01	0.01	0.11	0.01	0.00	0.00	<b>0.85</b>	<b>0.68</b>	0.01	0.05	1.0

\* Values of the determination coefficients,  $r^2$ , higher than 0.5 are presented in bold.

For the rate constant  $k$ , the best model equation obtained is the following:

$$\ln k = (0.70 \pm 0.04) + (0.30 \pm 0.06)V_{\text{micro}} - (1.06 \pm 0.09)S \quad (1)$$

(100%)                      (100%)                      (100%)

$$N = 13; R^2 = 0.940; R^2_{\text{adj}} = 0.928; s_{\text{fit}} = 0.09; F = 78 \quad (2)$$

where  $N$  is the number of points,  $s_{\text{fit}}$  is the standard deviation of fit,  $R^2$  is the determination coefficient,  $R^2_{\text{adj}}$  is the adjusted determination coefficient, and  $F$  is the Fisher–Snedecor ratio. The significance level in the percentage of each descriptor's coefficient is shown in brackets.

Considering that all descriptors were normalized, it is possible to say that  $\ln k$  increases with  $V_{\text{micro}}$ , the least important of the two descriptors, implying that these catalytic reactions occur mainly inside the micropores, meaning that mesopores are mainly important to enhance diffusion, in agreement with what was already reported in a previous work [19]. However, it is important to mention that there is a high correlation between  $V_{\text{micro}}$ ,  $C_{\text{XRD}}$ , and  $A_{\text{ext}}$  (Table 5), and thus it is not possible to evaluate independently the influence of each of these parameters on the kinetic constant.

With opposite and higher magnitude in the model equation is the  $S$  parameter. This parameter is also highly correlated with the  $E$  and  $V$  parameters. We can presume that dipolarity/polarizability ( $E$  and  $S$ ) decrease the rate constant since stronger substrate-zeolite interactions result in the occupancy of active sites thus decreasing the reaction rate. However, it is not possible to overlook that the negative substrate size effect may be also



included in the coefficient of the  $S$  parameter. It is interesting to note that, according to the above correlation, the increase in rate constant verified for benzofuran for desilicated and acid treated BEA zeolites (see Table 3) does not seem to be directly affected by the mesoporosity generation and acidity modifications that occurred as a consequence of the treatments. A possible reason lies in the fact that all substrates used in the correlation, including benzofuran, have molecular sizes that can fit the micropores of the BEA zeolite structure [23]. Nevertheless, the created mesoporosity has surely a positive impact on suppressing diffusion limitations that indirectly increase the reaction rate and improve the access to the active sites. Concerning the acidity, the absence of this property in Eq. 1 is not surprising since, as verified before, only a decrease of more than 50% in  $[B]_{\text{pyr}}$  led to an increase in  $k$  [19], meaning that this reaction is not particularly demanding regarding the amount and strength of acid sites.

For the adsorption related equilibrium constant,  $K_r$ , the best-found equation was:

$$\ln K_r = (0.36 \pm 0.03) + (0.67 \pm 0.08)S \quad (3)$$

$$(100\%) \quad (100\%)$$

$$N = 12; R^2 = 0.875; R^2_{\text{adj}} = 0.863; s_{\text{fit}} = 0.08; F = 70 \quad (4)$$

Results show no significant role of zeolite descriptors, and adsorption equilibrium is clearly driven by the  $S$  substrate parameter, with  $\ln K_r$  increasing with the substrate dipolarity/polarizability. This fact, already observed in our previous work (although using another parameter,  $E_T^N$ , which includes a dipolarity component), suggests an increase in product adsorption with substrate dipolarity/polarizability [19]. However, as mentioned above, the  $S$  parameter is also correlated with the substrate size, so, once again, the substrate size cannot be discarded, and its effect may be considered in the coefficient of the  $S$  parameter. The substrate size would have also a positive contribution on  $\ln K_r$ .

### 3. Materials and Methods

#### 3.1. Materials

In the present study, commercially available chemicals were used without further purification and were purchased from Merck (Darmstadt, Germany). The parent zeolite material was the BEA structure with a Si/Al = 12.5. According to the technical report of the supplier (Zeolyst, Farmsum, The Netherlands), the zeolite sample, Lot. CP814E, has a  $\text{Na}_2\text{O}$  weigh of 0.05% and a surface area of  $680 \text{ m}^2 \text{ g}^{-1}$ . The zeolite was supplied as  $\text{NH}_4\text{BEA}$  and was transformed into the protonic form through heat treatment under dry air ( $6 \text{ L h}^{-1} \text{ g}^{-1}$ ) at  $500 \text{ }^\circ\text{C}$  for 3 h.

#### 3.2. Preparation of the Hierarchical BEA Zeolite Samples

Hierarchical BEA samples were prepared through post-synthesis treatments using the methodology applied in our previous works [15,19,21]. In brief, the zeolite in its protonic form, herein designated as BEA, was submitted to an alkaline treatment with 0.2 or 0.4 M NaOH (p.a.), using a liquid/solid ratio of  $30 \text{ mL g}^{-1}$  for 30 min at  $60 \text{ }^\circ\text{C}$ , under vigorous stirring. The solid was recovered by centrifugation, washed, and dried. To account for some Na exchange during the alkaline treatment, the samples were reconverted to the protonic form by ion exchange with a 2 M  $\text{NH}_4\text{NO}_3$  (p.a.) solution using a liquid/solid relation of  $25 \text{ mL g}^{-1}$  at  $80 \text{ }^\circ\text{C}$  for 6 h. The solid was recovered using the same procedure described before, followed by calcination at  $500 \text{ }^\circ\text{C}$  for 3 h under dry air. The desilicated samples were further submitted to an acid treatment with 0.1 M HCl (p.a., fuming 37%), with a liquid/solid ratio of  $30 \text{ mL g}^{-1}$  at  $70 \text{ }^\circ\text{C}$  for 3 h. The solid was recovered as described above and the modified samples were designated as  $\text{BEA}_x$ , where “ $x$ ” corresponds to the NaOH concentration, followed by “AT” when the samples were submitted to acid treatment.

### 3.3. Physicochemical Characterization

Parent and hierarchical materials were characterized through several techniques; some of them were already thoroughly described in previous works [19,21]. The structural characterization was carried out using X-ray powder diffraction (Philips, Analytical PW 350/60 X'Pert PRO with X'Celerated detector, Almelo, The Netherlands). The diffractograms were acquired at room temperature using CuK $\alpha$  radiation as the incident beam, by continuous scanning from 5 to 40 ( $^{\circ}2\theta$ ), with a step size of 0.017  $^{\circ}2\theta$  and using a time per step of 20 s.

The  $^{29}\text{Si}$  magic-angle spinning (MAS) NMR spectra were recorded in a Bruker Avance III 400 NMR (9.4 T) (Bruker, Billerica, MA, USA) wide-bore spectrometer at 79.5 MHz on a double-resonance 7 mm Bruker probe with a 5 kHz spinning rate, 45 $^{\circ}$  radio-frequency (RF) pulses, and a 60 s recycle delay. The acquisition parameters for the  $^{29}\text{Si}$  cross-polarization MAS are: 1H and  $^{29}\text{Si}$  90 $^{\circ}$  pulses set to 2 and 6 ms, corresponding to a RF field strength of 125 and 42 kHz, respectively. The CP step was implemented using a contact time of 2 ms with a ramp shape in the 1H channel of 50–100% and  $^{29}\text{Si}$  RF field strength of 66 kHz. During the acquisition, SPINAL-64 decoupling with a RF field strength of 50 kHz (SPINAL basic pulse length of 9.5 ms) was employed. Chemical shifts are quoted in ppm from tetramethylsilane (TMS). The  $^{27}\text{Al}$  MAS NMR spectra were recorded on a Bruker Avance III HD (Bruker, Billerica, MA, USA) 700 MHz (16.4 T) narrow-bore spectrometer at 182.4 MHz on a double-resonance 4 mm Bruker probe with a 15 kHz spinning rate. Single quantum ('normal') spectra were recorded using a short RF pulse of 0.27  $\mu\text{s}$  (equivalent to a  $\pi/18$  flip angle), calibrated on an aqueous solution of  $\text{Al}(\text{NO}_3)_3$ , with 100 kHz field strength and 0.5 s recycle delay.

The textural characterization was carried out using  $\text{N}_2$  adsorption at  $-196^{\circ}\text{C}$  using an automatic apparatus Micromeritics ASAP 2010 (Micromeritics Instruments Corporation, Norcross, GA, USA). Prior to the isotherm measurement, the samples (around 50 mg) were outgassed at 300  $^{\circ}\text{C}$  for 3 h under vacuum higher than  $10^{-2}$  Pa. The micropore volume,  $V_{\text{micro}}$ , and external area,  $A_{\text{ext}}$ , were quantified by applying the  $\alpha_s$  method, using the standard isotherm obtained for non-porous silica as reference material [26]. The  $V_{\text{micro}}$  corresponds to the back extrapolation of the linear region of  $\alpha_s$  plot defined by the experimental points that correspond to  $\alpha_s > 1$ , whereas  $A_{\text{ext}}$  was obtained using the slope. The mesoporous volume,  $V_{\text{meso}}$ , was quantified from the difference between  $V_{\text{total}}$  and  $V_{\text{micro}}$ , where  $V_{\text{total}}$  is the total pore volume and corresponds to the  $\text{N}_2$  volume adsorbed at a relative pressure of 0.95, according to the Gurvitch rule [26]. The mesopore size distribution was obtained through Hybrid Density Functional Theory (DFT Plus<sup>®</sup> V2.01 for ASAP 2010 V5.00), assuming cylindrical pore shape. The acidity characterization was carried out using pyridine adsorption followed by FTIR spectroscopy using a Nicolet spectrophotometer (Thermo Fisher Scientific, Waltham, MA, USA). Initially, the samples (around 10 mg  $\text{cm}^{-2}$ ) were outgassed at 450  $^{\circ}\text{C}$  for 3 h (vacuum better than  $10^{-6}$  mbar). After evacuation, the wafers were cooled to room temperature, and the initial (base) spectrum was recorded. The wafers were then exposed to pyridine vapour ( $2.6 \times 10^2$  Pa) for 20 min for saturation at ambient temperature. After 2 h under vacuum for the evacuation of the physisorbed pyridine, the spectra were recorded (64 scans, resolution 4  $\text{cm}^{-1}$ ). The wafers were then heated for 1.5 h at 150  $^{\circ}\text{C}$  and, in a second step, to 350  $^{\circ}\text{C}$ . Then the spectra of chemisorbed pyridine were recorded. The background spectrum, recorded under identical operating condition, without sample, was always performed before each spectrum and automatically subtracted. The band intensities were corrected from slight differences in sample weight, band areas were calculated by fitting the spectral profiles with a Gaussian function using Peak-Fit<sup>®</sup> software and the concentration of acid sites was estimated according to Emeis [22].

### 3.4. Catalytic Experiments

The catalytic studies were performed in a three-necked round-bottom flask equipped with a reflux condenser, using a heating plate with temperature control (IKA C-MagHS7, Staufen, Germany). In a standard experiment, each of the substrates, furan (purity > 99%,

0.71 g, i.e., 10.5 mmol) or benzofuran (purity > 99%, 1.24 g, i.e., 10.5 mmol), were mixed with acetic anhydride as acylating agent (purity > 99%, 5.4 g, i.e., 52.5 mmol). In both cases, the ratio between substrate and acylating agent is equal to 5. The reagents were added to a sample of parent or modified BEA zeolite (150 mg). The suspensions were heated at 60 °C and, periodically, small aliquots were withdrawn from the reaction mixture using a hypodermic syringe and filtered with a membrane filter (Millipore Swinnex support with a Millipore Durapore 0.45 µm). Upon quenching in an ice bath, to “stop” the reaction, each aliquot was analyzed by gas chromatography using a Perkin Elmer Auto System (Perkin Elmer, Norwalk, CT, USA) equipped with a FID detector, using N<sub>2</sub> as carrier gas and a 30 m DB-5MS capillary column from Agilent (Santa Clara, CA, USA). All products and unconverted reactants were identified by comparison of the retention times with those of previously injected standard samples and the signals were integrated using DataApex CSW32 software (DataApex, Prague, Czech Republic).

### 3.5. Kinetic Studies

The Langmuir-Hinshelwood model is the kinetic model that best describes liquid phase reactions catalysed by porous materials. This model takes into consideration the competition between reactants and products for the active sites in the pores of the catalyst. In addition, the model admits that, although only one molecule can be adsorbed at the active sites, either reactants or products may block the access to the inner active sites [27,28]. The reaction scheme can be represented as:



where A is the acylating agent, S is the substrate, and P is the acylated product. Based on the methodology presented in our previous studies [18–20], the reaction rate,  $r$ , can be expressed after simplification as:

$$r \cong \frac{k[A][S]}{([A] + [S] + K_r[P])^2} \quad (6)$$

where  $k$  represents the rate constant of the rate determining step and  $K_r$  represents the ratio of the adsorption equilibrium constant of the product(s) and the normalized equilibrium constant of the reagents. The values of  $k$  and  $K_r$  as well as the corresponding statistical parameters are estimated through nonlinear regression using Table Curve 2D software 5.0.1.

## 4. Conclusions

In this study, BEA zeolite was modified through desilication or desilication and acid treatments, aiming to improve its catalytic performance in Friedel-Crafts acylation reactions using two substrates with the same functionality but distinct molecular sizes: furan and benzofuran. The characterization of the samples showed that textural and acidity modifications were obtained as a consequence of the treatments. The catalytic results showed different behaviors according to the molecular size of the substrate. In the case of furan, besides the high yields attained, all modified samples presented lower rate constants and TOFs when compared to the parent BEA zeolite. In the case of benzofuran, despite the low yields, the desilicated and acid treated samples showed higher  $k$  and TOFs, especially BEA0.2AT, meaning that the zeolite modifications had a positive impact when using larger molecules, as desired.

The correlations between  $\ln k$  and  $\ln K_r$  with different zeolite and substrate properties' descriptors using a QSPR methodology showed that the increase in rate constant,  $k$ , is positively influenced by  $V_{micro}$ , meaning that the catalytic reactions still occur mainly inside the micropores. However, it must be emphasized that the generated mesopores have an important role as transportation channels by lowering diffusional limitations, which indirectly increases the reaction rate. The results also indicate the role of stronger

substrate-zeolite interactions, assessed with the  $S$  parameter, which decreases the reaction rate. The relative sorption equilibrium constant,  $K_r$ , is affected by properties associated with the substrate, namely the  $S$  parameter, related to dipolarity/polarizability, as well as the substrate size.

In summary, this study led us to conclude that even when performing treatments in harsher conditions, using higher NaOH concentrations, the properties with a strong influence on the variation of the catalytic parameters are the same as those observed when the zeolite is treated using milder conditions, most probably because the substrate molecule benzofuran is still not large enough to duly probe the direct effect of mesopores, although this secondary pore system does have an important but indirect role as a transportation channel by reducing diffusion limitations.

**Supplementary Materials:** The following supporting information can be downloaded at: <https://www.mdpi.com/article/10.3390/catal12091064/s1>, Figure S1: Mesopore size distribution for parent and treated samples.

**Author Contributions:** Conceptualization and methodologies, A.M., A.P.C. and N.N.; validation, A.M., N.N., R.E.-L., F.M. and A.P.C.; formal analysis, R.E.-L., N.N., F.M., A.M., J.R. and A.F.; investigation, N.N., A.M. and A.F.; resources, F.M. and A.P.C.; writing—original draft preparation, A.M. and N.N.; writing—review and editing, R.E.-L., A.P.C. and F.M.; visualization, A.M. and N.N.; supervision, N.N. and A.M. All authors have read and agreed to the published version of the manuscript.

**Funding:** This research was funded by Fundação para a Ciência e a Tecnologia (FCT) through UIDB/00100/2020, UIDP/00100/2020, and LA/P/0056/2020, and Instituto Politécnico de Lisboa (IPL) through Project IPL/2021/ZeoGemini ISEL.

**Data Availability Statement:** Not applicable.

**Conflicts of Interest:** The authors declare no conflict of interest.

**Sample Availability:** Samples of the substrates and zeolites are available from the authors.

## References

1. Friedel, C.; Crafts, J.M. Sur une nouvelle méthode générale de de synthèse de hydrocarbures, d'acétones, etc. *Compt. Rendus* **1877**, *84*, 1392–1395.
2. Alshorifi, F.T.; Tobbala, D.E.; El-Bahy, S.M.; Nassan, M.A.; Salama, R.S. The role of phosphotungstic acid in enhancing the catalytic performance of UiO-66 (Zr) and its applications as an efficient solid acid catalyst for coumarins and dihydropyrimidinones synthesis. *Catal. Commun.* **2022**, *169*, 106479. [[CrossRef](#)]
3. Altass, H.M.; Khder, A.S.; Ahmed, S.A.; Morad, M.; Alsabei, A.A.; Jassas, R.S.; Althagafy, K.; Ahmed, A.I.; Salama, R.S. Highly efficient, recyclable cerium-phosphate solid acid catalysts for the synthesis of tetrahydrocarbazole derivatives by Borsche–Drechsel cyclization. *React. Kinet. Mech. Catal.* **2021**, *134*, 143–161. [[CrossRef](#)]
4. Guisnet, M.; Ribeiro, F.R. *Les zeolithes: Un Nanomonde au Service de la Catalyse*; EDP Science: Les Ullis, France, 2006; ISBN 978286838261.
5. Clerici, M.G. Zeolites for fine chemicals production. *Top. Catal.* **2000**, *13*, 373–386. [[CrossRef](#)]
6. Sartori, G.; Maggi, R. *Advances in Friedel-Crafts Acylation Reactions: Catalytic and Green Processes*; CRC Press: Boca Raton, FA, USA, 2009; ISBN 9781420067934.
7. Liang, J.; Liang, Z.; Zou, R.; Zhao, Y. Heterogeneous Catalysis in Zeolites, Mesoporous Silica, and Metal–Organic Frameworks. *Adv. Mater.* **2017**, *29*, 1–21. [[CrossRef](#)]
8. Nayak, Y.N.; Nayak, S.; Nadaf, Y.F.; Shetty, N.S.; Gaonkar, S.L. Zeolite Catalyzed Friedel-Crafts Reactions: A Review. *Lett. Org. Chem.* **2019**, *17*, 491–506. [[CrossRef](#)]
9. Cavani, F.; Centi, G.; Perathoner, S.; Trifiró, F. Sustainable Industrial Process. In *Principles, Tools and Industrial Examples*; Wiley: Weinheim, Germany, 2009; ISBN 978-3-527-31552-9.
10. Carvalho, A.P.; Nunes, N.M.A. Hierarchical Zeolites: Preparation, Properties and Catalytic Applications. In *Comprehensive Guide for Mesoporous Materials, Vol. 3: Properties and Development*; Aliofkhaezraei, M., Ed.; Nova Science Publishers: New York, NY, USA, 2015; pp. 147–211. ISBN 978-1-63463-318-5.
11. Derouane, E.G.; Schmidt, I.; Lachas, H.; Christensen, C.J.H. Improved performance of nano-size H-BEA zeolite catalysts for the Friedel-Crafts acetylation of anisole by acetic anhydride. *Catal. Lett.* **2004**, *95*, 13–17. [[CrossRef](#)]
12. Ji, X.; Qin, Z.; Dong, M.; Wang, G.; Dou, T.; Wang, J. Friedel-Crafts acylation of anisole and toluene with acetic anhydride over nano-sized Beta zeolites. *Catal. Lett.* **2007**, *117*, 171–176. [[CrossRef](#)]

13. Paixão, V.; Carvalho, A.P.; Rocha, J.; Fernandes, A.; Martins, A. Modification of MOR by desilication treatments: Structural, textural and acidic characterization. *Microporous Mesoporous Mater.* **2010**, *131*, 350–357. [[CrossRef](#)]
14. Fernandez, C.; Stan, I.; Gilson, J.P.; Thomas, K.; Vicente, A.; Bonilla, A.; Pérez-Ramírez, J. Hierarchical ZSM-5 zeolites in shape-selective xylene isomerization: Role of mesoporosity and acid site speciation. *Chem. A Eur. J.* **2010**, *16*, 6224–6233. [[CrossRef](#)]
15. Machado, V.; Rocha, J.; Carvalho, A.P.; Martins, A. Modification of MCM-22 zeolite through sequential post-synthesis treatments. Implications on the acidic and catalytic behaviour. *Appl. Catal. A Gen.* **2012**, *445–446*, 329–338. [[CrossRef](#)]
16. Verboekend, D.; Mitchell, S.; Milina, M.; Groen, J.C.; Javier, P. Full Compositional Flexibility in the Preparation of Mesoporous MFI Zeolites by Desilication. *J. Phys. Chem.* **2011**, *115*, 14193–14203. [[CrossRef](#)]
17. Wang, Y.; Sun, Y.; Lancelot, C.; Lamonier, C.; Morin, J.C.; Revel, B.; Delevoye, L.; Rives, A. Effect of post treatment on the local structure of hierarchical Beta prepared by desilication and the catalytic performance in Friedel-Crafts alkylation. *Microporous Mesoporous Mater.* **2015**, *206*, 42–51. [[CrossRef](#)]
18. Aleixo, R.; Elvas-Leitão, R.; Martins, F.; Carvalho, A.P.; Brigas, A.; Martins, A.; Nunes, N. Kinetic study of Friedel-Crafts acylation reactions over hierarchical MCM-22 zeolites. *Mol. Catal.* **2017**, *434*, 175–183. [[CrossRef](#)]
19. Aleixo, R.; Elvas-leitão, R.; Martins, F.; Carvalho, A.P.A.P.; Brigas, A.; Nunes, R.; Fernandes, A.; Rocha, J.; Martins, A.; Nunes, N. Zooming in with QSPR on Friedel-Crafts acylation reactions over modified BEA zeolites. *Mol. Catal.* **2019**, *476*, 110495. [[CrossRef](#)]
20. Elvas-Leitão, R.; Martins, F.; Borbinha, L.; Marranita, C.; Martins, A.; Nunes, N. Probing substrate/catalyst effects using QSPR analysis on Friedel-Crafts acylation reactions over hierarchical BEA zeolites. *Molecules* **2020**, *25*, 5682. [[CrossRef](#)]
21. Andrade, M.A.; Ansari, L.M.S.; Pombeiro, A.J.L.; Carvalho, A.P.; Martins, A.; Martins, L.M.D.R.S. Fe@hierarchical bea zeolite catalyst for mw-assisted alcohol oxidation reaction: A greener approach. *Catalysts* **2020**, *10*, 1029. [[CrossRef](#)]
22. Emeis, C.A. Determination of Integrated Molar Extinction Coefficients for Infrared Absorption Bands of Pyridine Adsorbed on Solid Acid Catalysts. *J. Catal.* **1993**, *141*, 347–354. [[CrossRef](#)]
23. Baerlocher, C.H.; Meier, W.M.; Olson, D.H. *Atlas of Zeolite Framework Types*, 5th ed.; Elsevier: Amsterdam, The Netherlands, 2001; ISBN 0444507019.
24. Guidotti, M.; Coustard, J.-M.; Magnoux, P.; Guisnet, M. Acetylation of aromatics over acid zeolites: Seeking a viable alternative to Friedel-Crafts catalysts. *Pure Appl. Chem.* **2007**, *79*, 1833–1838. [[CrossRef](#)]
25. Lu, J.Z.; Acree, W.E.; Abraham, M.H. Updated Abraham model correlations for enthalpies of solvation of organic solutes dissolved in benzene and acetonitrile. *Phys. Chem. Liq.* **2019**, *57*, 84–99. [[CrossRef](#)]
26. Gregg, S.J.; Sidney, J.; Sing, K.S.W.; Gregg, S.J.K.S.W.S. *Adsorption, Surface Area and Porosity*, 2nd ed.; Academic Press: London, UK, 1982; ISBN 0-12-300956-1.
27. Derouane, E.G.; Dillon, C.J.; Bethell, D.; Derouane-Abd Hamid, S.B. Zeolite catalysts as solid solvents in fine chemicals synthesis 1. Catalyst deactivation in the Friedel-Crafts acetylation of anisole. *J. Catal.* **1999**, *187*, 209–218. [[CrossRef](#)]
28. Derouane, E.G.; Crehan, G.; Dillon, C.J.; Bethell, D.; He, H.; Derouane-Abd Hamid, S.B. Zeolite catalysts as solid solvents in fine chemicals synthesis: 2. Competitive adsorption of the reactants and products in the Friedel-Crafts acetylations of anisole and toluene. *J. Catal.* **2000**, *194*, 410–423. [[CrossRef](#)]